

Nature and Raman signatures of the Higgs amplitude mode in the coexisting superconducting and charge-density-wave state

T. Cea^{*} and L. Benfatto[†]*ISC-CNR and Dep. of Physics, "Sapienza" University of Rome, P.le A. Moro 5, 00185, Rome, Italy*

(Received 28 July 2014; revised manuscript received 27 November 2014; published 18 December 2014)

We investigate the behavior of the Higgs (amplitude) mode when superconductivity emerges on a preexisting charge-density-wave state. We show that the weak overdamped square-root singularity of the amplitude fluctuations in a standard BCS superconductor is converted in a sharp, undamped power-law divergence in the coexisting state, reminiscent of the Higgs behavior in Lorentz-invariant theories. This effect reflects in a strong superconducting resonance in the Raman spectra, both for an electronic and a phononic mechanism leading to the Raman visibility of the Higgs. In the latter case, our results are relevant to the interpretation of the Raman spectra measured experimentally in NbSe₂.

DOI: [10.1103/PhysRevB.90.224515](https://doi.org/10.1103/PhysRevB.90.224515)

PACS number(s): 71.45.Lr, 74.20.-z, 74.25.nd

I. INTRODUCTION

The emergence of collective excitations after spontaneous breaking of a continuous symmetry is the mechanism at the heart of the mass generation for scalar and vector bosons in the standard model [1,2]. Its direct analogous in condensed matter physics is the appearance of two collective modes as fluctuations of the macroscopic (complex) order parameter in a superconducting (SC) system [3]. Indeed, amplitude fluctuations, which are energetically costly, represent the analogous of the Higgs field, and phase fluctuations, which are massless at long wavelengths, represent the Goldstone mode that can be gauged away to make the electromagnetic field massive, leading to the Meissner effect. Interestingly, the first experimental evidence of the Higgs particle [2] occurred simultaneously to a renewed interest in the literature on the behavior of the Higgs mode in condensed-matter systems [4], such as, e.g., superfluid cold atoms [5–9], where it can be excited by shaking the optical lattice [8,9].

On the other hand, in conventional BCS superconductors, the Higgs mode is usually very elusive, for two concomitant reasons. From one side, in contrast to Lorentz-invariant bosonic theories, in BCS superconductors the amplitude fluctuations do not identify a sharp power-law resonance, but only a weak square-root singularity at twice the SC gap Δ [10,11], that is strongly overdamped by quasiparticle excitations. Thus, even in a fully gapped superconductor, the Higgs-mode spectral function is a broad feature peaked exactly at the edge 2Δ where also single-particle excitations start to develop. In addition, in the weak-coupling BCS limit, the Higgs mode is expected to couple weakly to typical spectroscopic observables, like the current, probed by means of optical measurement, and the charge, probed by means of Raman spectroscopy. Indeed, the Higgs mode is a scalar, so it does not couple directly to the current, unless disorder breaks translational invariance [12], and it couples weakly to the charge, due to the intrinsic particle-hole symmetry enforced by the BCS solution. Thus, unless one strongly

perturbs the system out of equilibrium [13–15], the Higgs resonance remains hidden in conventional superconductors.

An exception to this rule seems to be the case of NbSe₂, a low-temperature superconductor ($T_c = 7$ K) where superconductivity emerges after a charge-density-wave (CDW) transition at higher temperature $T_{CDW} = 33$ K. In this material, a strong resonance in the Raman response [16,17] appears below T_c at about 2Δ . As suggested long ago within a phenomenological model by Littlewood and Varma [18], and within a more microscopic approach by Browne and Levin [19], this peak can be assigned to the Higgs mode. Indeed, according to this interpretation, the preexisting CDW state provides a soft phonon, Raman active already below T_{CDW} [20], that below T_c couples also to the Higgs mode. As a consequence, the phonon response itself carries out a signature of the SC amplitude mode, that becomes sharp since it is pushed slightly below the threshold 2Δ of quasiparticle excitations. In other words, the current theoretical understanding is that the preexisting CDW state is crucial to provide a mechanism of Raman visibility of the Higgs mode, but it does *not* change its nature.

This interpretation seems to be supported by the recent observation [17] that no sharp peak appears in the isostructural superconducting NbS₂, which lacks CDW order. On the other hand, the overall strength of the Higgs resonance in the experiments is much larger than what was predicted by the previous theoretical work [18,19], especially when one takes into account residual damping effects, neglected so far. In addition, the Higgs signature shows a still unexplained dependence on the Raman light polarization [17] that could be used instead to solve the still ongoing debate on the symmetry of the CDW and SC gaps in this material [21–25].

In this paper, we address the above issues by unveiling the real character of the Higgs fluctuations in the mixed CDW-SC state. As a first result, we show that in a CDW superconductor the CDW contributes crucially to modify the Higgs mode itself, making its detection easier whatever is the mechanism making it physically observable. By computing the Higgs mode in a microscopic CDW+SC model, we show that the presence of a CDW gap above the SC one pushes the quasiparticle continuum away from the Higgs pole at 2Δ , transforming the weak (overdamped) square-root singularity of a conventional BCS superconductor in a well-defined power-law divergence.

^{*}tommaso_cea@libero.it[†]lara.benfatto@roma1.infn.it

Thus, even in the weak-SC-coupling limit, the amplitude mode in the CDW+SC state resembles closely the one found in Lorentz-invariant relativistic theories, suitable in the bosonic limit [5–7]. This result has its own interest in the current discussion on the nature of Higgs fluctuations in condensed-matter systems, and it could be further tested by nonequilibrium spectroscopy, where a direct nonlinear coupling of the electromagnetic field to the amplitude mode can be generated [15]. Second, we compute explicitly the Raman response of the Higgs mode both in the absence and in the presence of an intermediate CDW phonon. In the former case, the coupling of the amplitude fluctuations to the Raman response is not zero when computed in a lattice mode, but still very small. While in an ordinary superconductor this would still lead to a negligible visibility of the strongly overdamped Higgs mode, in the CDW case the modified Higgs spectral function will emerge naturally as a strong resonance. In the case where a CDW phonon is also present the computation of the Raman response requires one to account for the intermediate electronic processes that make the CDW phonon itself Raman visible below T_{CDW} . This mechanism is analogous to the one discussed, e.g., for the Raman-active phonons in CDW dichalcogenides [26,27] or for the optical-active phonons in carbon-based compounds [28] and few-layer graphene [29–31]. When this effect is taken into account, one finds that the double-peak (phonon+Higgs) Raman structure emerging below T_c has in general a nontrivial temperature and polarization dependence. These results suggest that the recent observations of a polarization dependence of the Higgs signatures in the Raman spectra of NbSe₂ [17] can be used to disentangle the underlying symmetry of the two CDW and SC order parameters in this material.

The structure of the paper is the following. In Sec. II, we introduce the microscopic SC+CDW model and we compute the Higgs spectral function in the mixed state, showing its remarkable difference with the case of a conventional superconductor. In Sec. III, we analyze instead the Raman response, in the case where the CDW has an electronic (Sec. III A) or phononic (Sec. III B) origin. In both cases, we explain all the microscopic mechanisms making the Higgs and/or the phonon Raman visible, and we stress the effect of a modified Higgs mode on the Raman response. The final remarks are discussed in Sec. IV. In Appendix A, we discuss the differences and analogies between the coupling of the Higgs mode to the charge density and the Raman density, respectively. Finally, Appendix B contains some results for the present model away from half-filling to show the robustness of our conclusions in a regime where an analytical interpretation of the numerical results cannot be given.

II. HIGGS MODE IN THE COEXISTING CDW+SC STATE

As discussed in the Introduction, to make progress with respect to previous work [18,19] we need two ingredients: (i) an overlap between the SC and CDW gaps and (ii) a lattice model, crucial to account for the Raman-polarization effects. To minimize the resulting technical complications, we choose here a single-band model on the square lattice (lattice spacing $a = 1$) with band dispersion $\xi_{\mathbf{k}} \equiv \varepsilon_{\mathbf{k}} - \mu = -2t(\cos k_x + \cos k_y) - \mu$, where $t = 1$ is the hopping (that fixes the

energetic units from now on) and μ is the chemical potential. Near half-filling ($\mu = 0$), the nesting of the Fermi surface at the CDW vector $\mathbf{Q} = (\pi, \pi)$ allows for a CDW instability to occur, with new bands $\xi_{\pm} = -\mu \mp \sqrt{\varepsilon_{\mathbf{k}}^2 + D_0^2 \gamma_{\mathbf{k}}^2}$. Here, we model it with an order parameter $D_0 = W \sum_{\mathbf{k}\sigma} \langle \gamma_{\mathbf{k}} c_{\mathbf{k}\sigma}^\dagger c_{\mathbf{k}+\mathbf{Q}\sigma} \rangle$, where the $\gamma_{\mathbf{k}} = |\cos k_x - \cos k_y|$ factor modulates the CDW in the momentum space, so that below T_{CDW} the Fermi surface consists of small pockets around $(\pi/2, \pi/2)$. This feature is reminiscent of the situation in NbSe₂, where ARPES experiments [21–25] reported the presence of ungapped Fermi arcs below T_{CDW} . Here, the coupling W can be thought to originate either from an electronic interaction or from the coupling to a phonon, as we shall discuss in Sec. II B. The superconductivity originates from a BCS-type interaction term $H_{\text{SC}} = -(U/N) \sum_{\mathbf{q}} \Phi_{\Delta}^{\dagger}(\mathbf{q}) \Phi_{\Delta}(\mathbf{q})$, where $\Phi_{\Delta}(\mathbf{q}) \equiv \sum_{\mathbf{k}} c_{-\mathbf{k}+\mathbf{q}/2\downarrow} c_{\mathbf{k}+\mathbf{q}/2\uparrow}$ is the pairing operator and N is the number of lattice sites. When treated at mean-field level it leads to the following Green's function $G_0^{-1}(\mathbf{k}, i\omega_n)$, defined on the basis of a generalized 4-component Nambu spinor $\Psi_{\mathbf{k}}^{\dagger}(i\omega_n) \equiv [c_{\mathbf{k}\uparrow}^{\dagger}(i\omega_n), c_{\mathbf{k}+\mathbf{Q}\uparrow}^{\dagger}(i\omega_n), c_{-\mathbf{k}\downarrow}(-i\omega_n), c_{-\mathbf{k}-\mathbf{Q}\downarrow}(-i\omega_n)]$ that accounts for the CDW band folding:

$$G_0^{-1}(\mathbf{k}, i\omega_n) \equiv i\omega_n - \begin{pmatrix} \hat{h} & -\Delta_0 \sigma_0 \\ -\Delta_0 \sigma_0 & -\hat{h} \end{pmatrix}, \quad (1)$$

where Δ_0 is the SC gap, σ_i denotes the Pauli matrices, and \hat{h} is a 2×2 matrix:

$$\hat{h} = \begin{pmatrix} \varepsilon_{\mathbf{k}} - \mu & -D_0 \gamma_{\mathbf{k}} \\ -D_0 \gamma_{\mathbf{k}} & -\varepsilon_{\mathbf{k}} - \mu \end{pmatrix}. \quad (2)$$

The eigenvalues of the matrix \hat{h} represent the two CDW bands ξ_{\pm} , while in the SC state the full Green's function (1) has four possible poles, corresponding to the energies $\pm E_{\pm}(\mathbf{k})$, with $E_{\pm} = \sqrt{\xi_{\pm}^2 + \Delta_0^2}$. We note in passing that a similar model (but with d -wave symmetry of the SC order parameter) has been the subject of intense investigation in the past within the context of cuprate superconductors, as a potential model for a CDW-like pseudogap phase [32].

To study the SC fluctuations, we derive the effective action for the collective modes by means of the usual Hubbard-Stratonovich decoupling of H_{SC} [33]. After integration of the fermions, one is left with an action $S = S_{\text{MF}} + S_{\text{FL}}$ for the collective SC degrees of freedom only, where $S_{\text{MF}} = N\Delta_0^2/TU - \text{Tr} \ln G_0^{-1}$ is the mean-field action and $S_{\text{FL}}[\Delta, \theta]$ is the action for the amplitude Δ and phase θ fluctuations around the BCS solution (1) above. With respect to the usual case here the presence of a CDW instability introduces in general in S_{FL} a finite coupling between the SC fluctuations at \mathbf{q} and $\mathbf{q} + \mathbf{Q}$ (see Appendix B). However, one can show that this coupling vanishes at half-filling, so for the sake of simplicity we will discuss in the following this case. At the same time, in the SC+CDW state, the amplitude and phase/charge fluctuations remain decoupled at Gaussian level, as it occurs in the usual weak-coupling SC state [18,33], so we can neglect them in what follows (see also discussion in Appendix A). The Gaussian action for the amplitude SC

fluctuations then reads as

$$S_{\text{FL}} = \frac{1}{2} \sum_q \left(\frac{2}{U} + \chi_{\Delta\Delta}(q) \right) |\Delta(q)|^2, \quad (3)$$

where $\chi_{\Delta\Delta}$ is the response function for the amplitude operator Φ_Δ and $q = (\mathbf{q}, \Omega_n)$, with Ω_n bosonic Matsubara frequencies. The behavior of the amplitude fluctuations is controlled by the function $X_{\Delta\Delta} \equiv 2/U + \chi_{\Delta\Delta}$ in Eq. (3) since $\langle |\Delta(q)|^2 \rangle = 1/X_{\Delta\Delta}$. In analogy with the usual SC case [11], one can replace the term $2/U = 2 \sum_{\mathbf{k}} \tanh(\beta E_{\mathbf{k}}/2)/E_{\mathbf{k}}$ by means of the self-consistent equation for Δ_0 , in order to get

$$X_{\Delta\Delta} = \frac{2}{U} + \chi_{\Delta\Delta} = \frac{2}{N} \sum_{\mathbf{k}} \frac{(i\Omega_n)^2 - 4\Delta_0^2}{E_{\mathbf{k}}[(i\Omega_n)^2 - 4E_{\mathbf{k}}^2]} \tanh(\beta E_{\mathbf{k}}/2), \quad (4)$$

where the summation is restricted to the reduced Brillouin zone and $E_{\mathbf{k}} = E_{\pm} = \sqrt{\varepsilon_{\mathbf{k}}^2 + \Delta_0^2 + D_0\gamma_{\mathbf{k}}^2}$. In first approximation one can estimate the integral (4) at $T = 0$ by assuming that both the density of states N_0 and the CDW gap are constant [i.e., $\gamma_{\mathbf{k}} = 1$]. In this case, one can easily obtain that, for $\omega \lesssim 2\Delta_0$,

$$X'_{\Delta\Delta} \simeq (4\Delta_0^2 - \omega^2) \frac{N_0 \text{atan}(\Delta_0/D_0)}{\omega \sqrt{4D_0^2 + 4\Delta_0^2 - \omega^2}}. \quad (5)$$

In the pure SC case ($D_0 = 0$), the denominator diverges as a square root at $\omega = 2\Delta_0$ [11], signaling the proliferation of single-particle excitations above this threshold, and $X'_{\Delta\Delta} \sim \sqrt{4\Delta_0^2 - \omega^2}$ near the Higgs mass $\omega = 2\Delta_0$. In contrast, in the mixed state the CDW gap pushes the quasiparticle continuum away from the Higgs mode, leading to a finite denominator in Eq. (5). This implies a *linear* vanishing of $X'_{\Delta\Delta}$ at $2\Delta_0$ and suppresses its imaginary part $\Gamma_\Delta \equiv -X''_{\Delta\Delta}$. These simple estimates are confirmed by the numerical calculation done for the real band dispersion, as shown in Figs. 1(a) and 1(b), where we report both $X'_{\Delta\Delta}$ and Γ_Δ in the two cases, with and without preformed CDW state. To account also for residual quasiparticle scattering, we added a finite constant broadening γ in the response functions. As one can see in Fig. 1(a), in the SC+CDW state $X'_{\Delta\Delta}$ vanishes approximately linearly, in

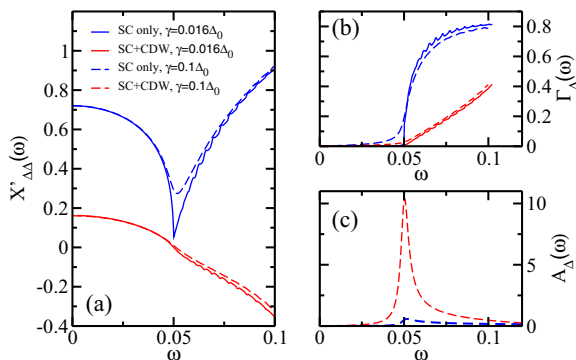


FIG. 1. (Color online) Frequency dependence of the real (a) and imaginary (b) parts of the Higgs spectral function (c) at $T = 0$ in the presence (SC+CDW) and in the absence (SC only) of CDW, for a quasiparticle damping $\gamma = 0.016\Delta_0$ (solid lines) and $\gamma = 0.1\Delta_0$ (dashed lines). Here, $\Delta_0 = 0.025$, as in Fig. 2.

contrast to the square root of the usual SC case [11] computed with the same Δ_0 , and Γ_Δ [see Fig. 1(b)] develops smoothly above $2\Delta_0$ since only few quasiparticle excitations in the regions with small CDW gap contribute to it. These two concomitant effects lead to a dramatic sharpening of the Higgs spectral function $A_\Delta(\omega) = (1/\pi)\text{Im}X_{\Delta\Delta}^{-1}(i\Omega_n \rightarrow \omega + iO^+)$

$$A_\Delta \equiv \frac{1}{\pi} \frac{\Gamma_\Delta(\omega)}{X_{\Delta\Delta}^2(\omega) + \Gamma_\Delta^2(\omega)}, \quad (6)$$

shown in Fig. 1(c) for the case $\gamma = 0.1\Delta_0$. While in the ordinary SC state we recover the typical overdamped structure of the amplitude fluctuations, in the CDW+SC state the Higgs mode becomes a well-defined excitation, rather insensitive to residual quasiparticle excitations, that are pushed away from the Higgs pole by the CDW gap. As we show in Appendix B, the same qualitative features survive also at finite doping, even if part of the Fermi surface remains ungapped below T_{CDW} . The strong modifications of the Higgs spectral function shown in Fig. 1(c), due to the emergence of superconductivity on the preexisting CDW state, represent the first crucial result of our work. Indeed, they imply that whatever is the mechanism that couples the Higgs mode to a physical observable, its detection in the mixed state becomes easier since the mode itself is much sharper than in an ordinary superconductor. As an example of this mechanism, we will discuss in the next section the case of the Raman response.

III. RAMAN SIGNATURES OF THE HIGGS MODE

A. Electronic mechanism

We first compute the Raman spectra in the case where the CDW has an electronic origin, so that the Raman visibility of the Higgs can only be due to a direct coupling between the SC amplitude fluctuations and the Raman charge fluctuations. Within the effective-action formalism, the Raman response can be computed by introducing in the fermionic model a source term ρ_R coupled to the Raman density operator $\Phi_R(\mathbf{q}) \equiv \sum_{\mathbf{k}\sigma} \Gamma(\mathbf{k}) c_{\mathbf{k}-\mathbf{q}/2,\sigma}^\dagger c_{\mathbf{k}+\mathbf{q}/2,\sigma}$. Here, $\Gamma(\mathbf{k})$ is the Raman vertex, determined by the polarization of the incident and scattered photon [34]. After integration of the fermions, ρ_R appears as an additional bosonic field in the action S_{FL} , that now reads as

$$S_{\text{FL}} = \frac{1}{2} \sum_q \left\{ \left(\frac{2}{U} + \chi_{\Delta\Delta}(q) \right) |\Delta(q)|^2 + 2\rho_R(q)\Delta(-q)\chi_{R\Delta}(q) + |\rho_R(q)|^2\chi_{RR}^0(q) \right\}. \quad (7)$$

Here, $\chi_{AB}(q)$ denotes the response functions computed with the A, B operators, where R identifies the Raman density Φ_R , Δ the pairing operator Φ_Δ , and χ_{RR}^0 represents the BCS Raman response function in the absence of the collective modes. Notice that even if one included explicitly the Coulomb forces the Raman response here would be unaffected since phase fluctuations do not couple to the Raman response at $\mathbf{q} = 0$, while charge fluctuations, that in general screen χ_{RR}^0 in the symmetric A_{1g} channel [34], are ineffective in the present model since the charge-Raman coupling vanishes exactly at half-filling because of particle-hole symmetry. Finally,

the Raman response is obtained by analytical continuation $i\Omega_n \rightarrow \omega + i0^+$ as $S_R = -\frac{1}{\pi}[1 + n(\omega)]\chi''_{RR}(\mathbf{q} = 0, \omega)$, where $n(\omega)$ is the Bose-Einstein distribution and χ_{RR} is the Raman susceptibility, computed from Eq. (7) as

$$\chi_{RR}(q) = \left[\frac{\delta^2 S_{\text{FL}}}{\delta\rho_R(-q)\delta\rho_R(q)} \right]_{\rho_R=0}. \quad (8)$$

By integrating out explicitly the amplitude fluctuations in Eq. (7), we are then left with the Raman response

$$\chi_{RR} = \chi_{RR}^0 - \chi_{R\Delta}^2 / X_{\Delta\Delta}, \quad (9)$$

where the second term, depicted in Fig. 3(a), is equivalent to compute the random phase approximation (RPA) vertex corrections due to amplitude fluctuations [34]. The coupling of the Higgs to the Raman density is mediated by the fermionic susceptibility $\chi_{R\Delta}$:

$$\chi_{R\Delta} = \frac{8\Delta_0}{N} \sum_{\mathbf{k}} \frac{\Gamma(\mathbf{k})\varepsilon_{\mathbf{k}} \tanh(\beta E_{\mathbf{k}}/2)}{E_{\mathbf{k}}[(i\Omega_n)^2 - 4E_{\mathbf{k}}^2]}, \quad (10)$$

that is finite in the A_{1g} channel where $\Gamma(\mathbf{k}) = (\cos k_x + \cos k_y) \propto \varepsilon_{\mathbf{k}}$. Since in the A_{1g} channel the BCS contribution χ_{RR}^0 is negligible, for this symmetry the Raman response probes essentially the spectral function A_{Δ} of the Higgs mode given by Eq. (6):

$$\chi''_{RR} \simeq \pi \chi_{R\Delta}^2(\omega) A_{\Delta}(\omega), \quad (11)$$

leading to the results of Fig. 2 for the CDW+SC (solid lines) and SC only (dashed lines) case. As we discuss in detail in the Appendix A, the coupling $\chi_{R\Delta}$ of the Raman response to the Higgs is in general different from the coupling of the real charge density to SC amplitude fluctuations, that vanishes at weak coupling due to the approximate particle-hole symmetry of the BCS solution [18,33]. On the other hand, in an ordinary SC state even if this is a finite quantity it multiplies a strongly overdamped Higgs spectral function [see dashed lines in Fig. 1(c)], so the overall Raman signature of the Higgs is the broad and weak feature represented by dashed lines in Fig. 2. This justifies on microscopic grounds the general expectation [4] that the Higgs mode is irrelevant in

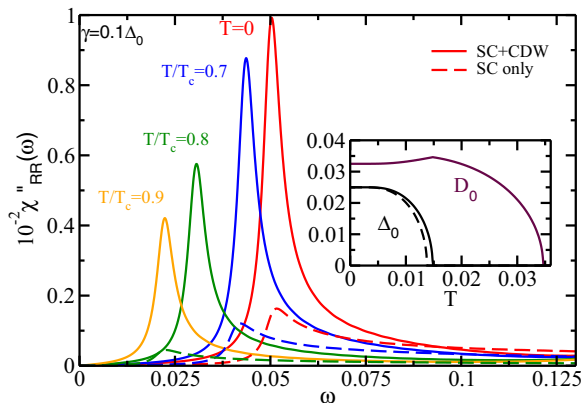


FIG. 2. (Color online) Electronic Raman response in the A_{1g} channel in the coexisting (solid lines) and pure (dashed lines) SC state as a function of temperature. Inset: temperature evolution of the SC gaps Δ_0 and of the CDW gap D_0 .

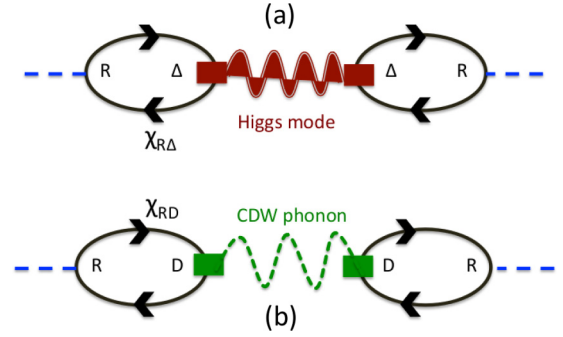


FIG. 3. (Color online) Feynman diagrams representing the electronic processes responsible for the Raman visibility of (a) the Higgs mode when $g = 0$ and (b) the CDW phonon above T_c . Here, the dashed lines represent the incoming electromagnetic radiation, the full lines the electronic Green's functions G_0 , the red and green wavy lines the Higgs propagator $X_{\Delta\Delta}^{-1}(\omega)$ and the phonon one $D(\omega)$, respectively. In the coexistence state for $g \neq 0$ the two processes become interconnected since both the phonon propagator [see Eq. (15)] and the χ_{RD} [see Eq. (17)] are renormalized by the coupling between the Higgs fluctuations and the CDW amplitude fluctuations.

the Raman spectra of an ordinary superconductor. However, in a CDW+SC state the situation is radically different since the spectral function itself of the Higgs mode is sharper than usual. Thus, even if in the coexisting state the $\chi_{R\Delta}$ prefactor in Eq. (11) is smaller than in the usual SC state (see Appendix B), the modifications of the Higgs spectral function $A_{\Delta}(\omega)$ shown in Fig. 1 lead to the sharp resonance at $2\Delta_0(T)$ shown in Fig. 2. In other words, the CDW state is not modifying the mechanism coupling the Higgs to the Raman probe, but it is changing dramatically the nature of the Higgs mode itself, making it detectable.

B. Phononic mechanisms

A second possible mechanism that makes the Higgs mode visible in Raman is the one proposed long ago in the case of NbSe₂ [18,19], where Higgs fluctuations come along with the CDW phonon. To explore also this possibility we then consider the case where the CDW instability is driven by the microscopic coupling of the electrons to a phonon of energy ω_0 , $H_I = g \sum_{\mathbf{k}\sigma} \gamma_{\mathbf{k}} c_{\mathbf{k}+\mathbf{Q}\sigma}^\dagger c_{\mathbf{k}\sigma} (b_{\mathbf{Q}}^+ + b_{-\mathbf{Q}})$, so that $4g^2/\omega_0$ is equivalent to the coupling W used so far. At mean-field level, the description of the CDW+SC state is then identical to the one of Sec. II, and the SC amplitude fluctuations are described by the same effective action (3) derived above, leading to the results of Fig. 1. However, in the calculation of the Raman spectra, we should account for two additional effects: (i) the Raman response of the CDW phonon itself [26,27] and (ii) the coupling between the phonon and the Higgs, that reflects in a renormalization of the phonon propagator [18,19]. Since all these issues have been discussed only in part in the previous literature, we will outline the basic steps leading to the calculation of the Raman response in this case.

Let us first focus on the regime below T_{CDW} but above T_c . When the CDW is driven by a lattice instability, the energy ω_0 of the phonon is renormalized to the value Ω_0 by the amplitude

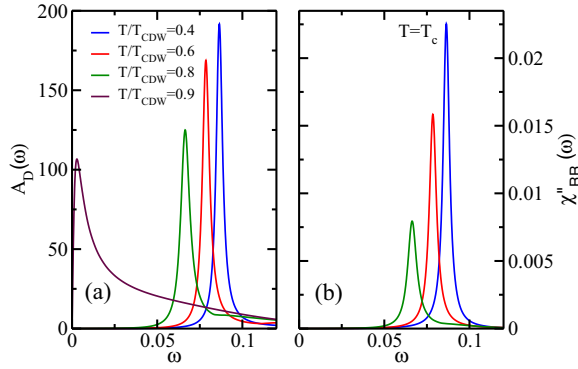


FIG. 4. (Color online) Temperature evolution of the phonon spectral function (a) and of the Raman response (b) of the CDW phonon between T_{CDW} and $T_c = 0.4T_{CDW}$.

fluctuations of the CDW [35]. The renormalized phonon propagator below T_{CDW} is then $D^{-1}(i\Omega_n) = -(\Omega_n^2 + \Omega_0^2)/2\omega_0$ with

$$\begin{aligned} \Omega_0^2 &= \omega_0^2 \left[1 + \frac{2g^2}{\omega_0} \chi_{DD} \right] \\ &= \frac{4g^2\omega_0}{N} \sum_{\mathbf{k}} \gamma_{\mathbf{k}}^2 \frac{(i\Omega_n)^2 - 4D_0^2\gamma_{\mathbf{k}}^2}{E_{\mathbf{k}}[(i\Omega_n)^2 - 4E_{\mathbf{k}}^2]} \tanh(\beta E_{\mathbf{k}}/2), \end{aligned} \quad (12)$$

where, in accordance to our notation, the subscript D labels the CDW amplitude operator $\Phi_D = \sum_{\mathbf{k}\sigma} \gamma_{\mathbf{k}}(c_{\mathbf{k}\sigma}^\dagger c_{\mathbf{k}+\mathbf{Q}\sigma} + \text{H.c.})$. The second line of Eq. (12) has been derived by using the self-consistency equation for the CDW gap, i.e., $1 = (4g^2/\omega_0 N) \sum_{\mathbf{k}} [\gamma_{\mathbf{k}}^2 \tanh(\beta E_{\mathbf{k}}/2)]/E_{\mathbf{k}}$. By comparison with Eq. (4), one sees that Ω_0^2 scales as the inverse propagator of the CDW amplitude fluctuations, that is itself massless at about $4D_0$ (where the additional factor of 2 comes from the $\gamma_{\mathbf{k}}$ modulation factor). As a consequence, the renormalized phonon energy also follows the T dependence of the CDW order parameter, so it vanishes at $T = T_{CDW}$ and it is reduced with respect to ω_0 at $T = 0$ [35], as shown by the phonon spectral function $A_D(\omega) = -(1/\pi)\text{Im}D(i\Omega_n \rightarrow \omega + i\delta)$ reported in Fig. 4(a). Notice that, in contrast to previous work [19,35], we retained here the full frequency dependence of Ω_0 , crucial as T increases and $D_0 \rightarrow 0$. Thus, the pole of the phonon propagator is determined self-consistently after analytical continuation as a solution of the equation $\omega^2 - \Omega_0^2(\omega) = 0$.

The formation of the CDW state is also responsible for the Raman visibility of the phonon. Indeed, in analogy with what is suggested for CDW dichalcogenides [26,27], the particle-hole excitations at $\mathbf{q} = 0$ probed by Raman couple to the electronic CDW fluctuations at \mathbf{Q} , that in turn can decay in a phonon, as depicted by the process of Fig. 3(b). The Raman response of the phonon above T_c is then given by

$$\chi_{RR}(i\Omega_n) = -g^2 \chi_{RD}^2 D(i\Omega_n) = -\frac{2g^2\omega_0 \chi_{RD}^2}{\Omega_0^2 - (i\Omega_n)^2}, \quad (13)$$

where

$$\chi_{RD} = 8D_0 \sum_{\mathbf{k}} \frac{\Gamma(\mathbf{k})\gamma_{\mathbf{k}}^2 \varepsilon_{\mathbf{k}}}{E_{\mathbf{k}}[(i\Omega_n)^2 - 4E_{\mathbf{k}}^2]} \tanh(\beta E_{\mathbf{k}}/2). \quad (14)$$

In full analogy with the case of the χ_{RD} function that makes the Higgs mode Raman visible, the χ_{RD} susceptibility depends on the combined symmetry of the Raman polarization, controlled by $\Gamma(\mathbf{k})$, the lattice structure, and the CDW symmetry. In the present case, one can easily see that Eq. (14) is different from zero only in the A_{1g} channel, where $\Gamma(\mathbf{k}) \propto \varepsilon_{\mathbf{k}}$. Since χ_{RD} scales as the CDW order parameter D_0 , the overall temperature evolution of the Raman response (13) of the phonon, shown in Fig. 4(b), differs considerably from the one of the spectral function. Indeed, as $T \rightarrow T_{CDW}$ the χ_{RD} vanishes rapidly [see inset of Fig. 6(a)] and the Raman response is completely suppressed, in agreement with the experimental observation in NbSe₂ [20]. It is also worth noting that the crucial role played by the intermediate particle-hole excitations to control the spectroscopic visibility of a phonon is a well-known effect in the literature. For example, in the context of optical conductivity, this is the so-called charged-phonon effect, originally introduced by Rice for carbon-based compounds [28], and widely discussed in the last few years within the context of few-layer graphene [29–31]. In this case, it has been shown that the strong doping dependence of the phonon-peak intensity and its Fano-type shape [29,30] can be explained by computing the optical visibility of the phonon coming from the process analogous to the one depicted in Fig. 3, with the Raman vertex replaced in this case by the current vertex [31].

Below T_c , the opening of the SC gap modifies both the Raman response, that now includes also the contribution (9) of the Higgs mode, and the phonon propagator itself, that gets renormalized by the SC amplitude fluctuations [18,19]. The latter mechanism was proposed originally by Littlewood and Varma (LV) [18], who introduced a phenomenological coupling g_{Δ} between the Higgs and the phonon. By following the language of LV, one can then write the phonon propagator D in the mixed state as $D^{-1}(\Omega_n) = -\frac{\Omega_n^2 + \tilde{\Omega}_0^2}{2\Omega_0}$, where $\tilde{\Omega}_0^2 = \Omega_0^2[1 - 2\Sigma_{\Delta}/\Omega_0]$ is the phonon energy renormalized by the coupling of the phonon to Higgs fluctuations, so that $\Sigma_{\Delta}(\omega) = -2g_{\Delta}^2 \chi_{\Delta\Delta}(\omega)/U X_{\Delta\Delta}$. Since near $2\Delta_0$ one has $\chi'_{\Delta\Delta} \simeq -2/U$ while $X'_{\Delta\Delta} \rightarrow 0$, as shown in Fig. 1, the pole of the phonon propagator determined as usual by $\omega^2 - \tilde{\Omega}_0^2(\omega) = 0$ has a new solution around the frequency of the Higgs mode [see Figs. 5(a) and 5(c)]. Once more the nature of the Higgs, encoded in $X'_{\Delta\Delta}$ and $\Gamma_{\Delta\Delta}$, gives qualitative and quantitative differences if one applies the above phenomenological approach by using the standard form of the Higgs fluctuations, as done by LV, or the real one in the coexisting SC+CDW state. These differences are elucidated in Fig. 5, where we show the renormalized phonon frequency $\tilde{\Omega}_0$ and the phonon spectral function for two values of the phenomenological coupling g_{Δ} and a residual phonon broadening $\delta = 0.1\Delta_0$ above T_c . Here, the Higgs fluctuations in the two cases (SC and SC+CDW) correspond to the calculations shown in Fig. 1 for $\gamma = 0.1\Delta_0$. As one can see, for the same remaining parameters, a weak feature found for conventional Higgs fluctuations turns out in a strong feature when the Higgs is computed in the mixed state [37]. Notice that the crucial role of the residual damping γ has been neglected so far [18,19], while it is certainly present in real materials and suppresses the signature of a conventional Higgs mode even when the coupling to the phonon moves it inside the

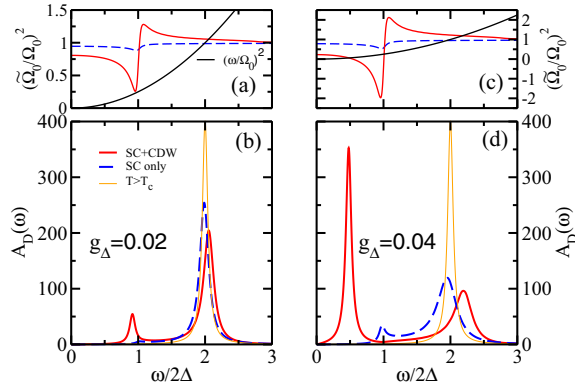


FIG. 5. (Color online) Renormalization of the phonon frequency (a), (c) and of the phonon spectral function A_D (b), (d) due to the Higgs mode according to the phenomenological approach by LV [18], where the phonon self-energy is $\Sigma_\Delta = -2g_\Delta^2 \chi_{\Delta\Delta}/U X_{\Delta\Delta}$. The Higgs fluctuations $X_{\Delta\Delta}$ are computed in the two cases, with (solid red lines) or without (dashed blue lines, as done in Ref. [18]) a preformed CDW, and correspond to the data of Fig. 1 for $\gamma = 0.1\Delta_0$. Here, the CDW phonon has energy $\Omega_0 = 4\Delta_0$ and $\delta = 0.1\Delta_0$, leading to the spectral function at $T > T_c$ shown by the thin orange line in panels (b) and (d). When entering the SC phase, the phonon peak at Ω_0 gets broader and slightly displaced, while a second peak develops below $2\Delta_0$ due to the Higgs self-energy Σ_Δ , that causes a second intersection for the curve $\omega^2 - \tilde{\Omega}_D^2$ in the inverse phonon propagator.

quasiparticle continuum. Thus, already this phenomenological approach shows that it is crucial to retain the real nature of the Higgs mode in the coexisting state in order to explain the strong signatures observed experimentally [17].

As shown later on by Browne and Levin (BL), the effective coupling g_Δ between the phonon and the Higgs arises microscopically from the coupling between the amplitude fluctuations of both the CDW and SC order parameters, so that the phonon propagator below T_c reads as

$$D^{-1}(i\Omega_n) = -\frac{\Omega_0^2 - (i\Omega_n)^2 - 2g^2\omega_0\chi_{D\Delta}^2/X_{\Delta\Delta}}{2\omega_0}, \quad (15)$$

where the function

$$\chi_{D\Delta} = -8D_0\Delta_0 \sum_{\mathbf{k}} \frac{\gamma_{\mathbf{k}}^2}{E_{\mathbf{k}}[(i\Omega_n)^2 - 4E_{\mathbf{k}}^2]} \tanh(\beta E_{\mathbf{k}}/2) \quad (16)$$

is the one that mediates the effective coupling between the phonon and the Higgs fluctuations. It is worth noting that in their paper, BL use a model where the SC and CDW order parameters coexist only on some fraction η (γ in the notation of Ref. [19]) of the Fermi surface. In the limit when $\eta \rightarrow 0$, BL notice that their result reproduces the one by LV: indeed, in this limit the Higgs mode is the standard one since in Eq. (5) above there is no CDW gap above the SC one to push the quasiparticle continuum away from the Higgs pole. When instead η increases, BL observe some numerical difference with respect to the results of LV, that they incorrectly attribute to a larger value of the effective coupling to the phonon, i.e., the function $\chi_{D\Delta}$ in Eq. (16). However, this is not the case: indeed, even if a larger overlap between the SC and CDW order parameters leads to an increase of $\chi_{D\Delta}$, the stronger effect in the formation of the coexistence state is in the profound

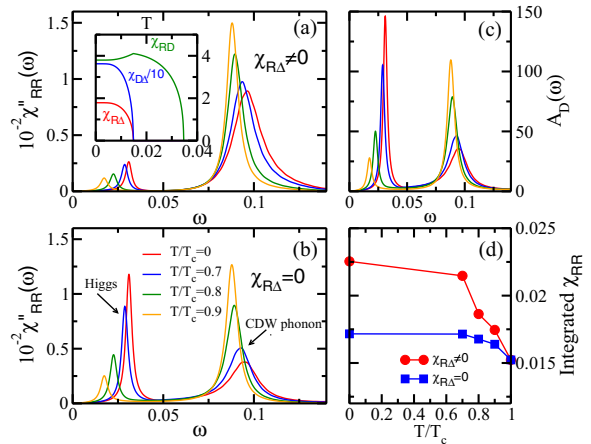


FIG. 6. (Color online) Raman response in the A_{1g} channel in the mixed CDW+SC state according to Eq. (17), both in the presence (a) and in the absence (b) of the direct Raman coupling to the Higgs, encoded in $\chi_{R\Delta}$. The double-peak structure found below T_c in the phonon spectral function, shown in panel (c) is weighted in the Raman response by the two polarization functions $\chi_{R\Delta}$ and χ_{RD} . Their value at $\omega = 0$ is shown in the inset of panel (a), along with the coupling $\chi_{D\Delta}$ between the two order parameters responsible for the Higgs signature in the phonon mode. (d) Temperature evolution of the Raman spectral weight integrated between $\omega = 0$ and 0.15 , for the two cases of panels (a) and (b).

modification of the Higgs spectral function. This is clearly shown in Fig. 5, where the two cases (Higgs mode computed with or without the CDW gap) are compared by keeping the same effective coupling g_Δ of the phonon to the Higgs.

Once clarified the role of the modified Higgs fluctuations on the phonon spectral function, we now present the results for the Raman response in the coexisting state. As one can easily see, the coupling (16) between the two order parameters renormalizes also the intermediate process χ_{RD} making the phonon Raman visible, so that the full Raman response reads as

$$\chi_{RR} = -\frac{\chi_{R\Delta}^2}{X_{\Delta\Delta}} - \frac{2g^2\omega_0[\chi_{RD} - \frac{\chi_{R\Delta}\chi_{D\Delta}}{X_{\Delta\Delta}}]^2}{\Omega_0^2 - (i\Omega_n)^2 - 2g^2\omega_0\chi_{D\Delta}^2/X_{\Delta\Delta}}, \quad (17)$$

where the first term corresponds to the response (9) of the Higgs alone and the second one accounts for the response (13) of the phonon mode, renormalized by the Higgs fluctuations according to Eq. (15). The temperature evolution of the Raman spectra is shown in Fig. 6(a) for the Δ_0 , D_0 appearing in Figs. 1 and 2. In agreement with the discussion above, the phonon spectral function, shown in Fig. 6(c), shows a double-peak structure evolving with temperature, one around Ω_0 and one below $2\Delta_0$, that is the signature of the Higgs mode. However, the way these two peaks appear in the Raman response depends crucially on the polarization functions χ_{RD} and $\chi_{R\Delta}$ [see Figs. 6(a) and 6(b)]. In particular, by comparing the results of Fig. 6(a) with the ones in Fig. 6(b), where we put by hand $\chi_{R\Delta} = 0$, one sees that the direct coupling $\chi_{R\Delta}$ of the Higgs to the light is crucial to establish the Raman spectral-weight distribution below T_c . Indeed, when $\chi_{R\Delta} = 0$ the Higgs feature at $T = 0$ is stronger than in the case of $\chi_{R\Delta} \neq 0$, shown in Fig. 6(a), and the broadening of the phonon peak is also

smaller. Both effects are due to the vanishing of the second term in square brackets of Eq. (17), that partly screens out the response at the Higgs when present. Nonetheless, the increase of the Raman spectral weight integrated up to $\omega \simeq 0.15$, shown in Fig. 6(d), is larger when $\chi_{R\Delta} \neq 0$, due to a larger broadening of the phonon in this case. Notice also that from Eq. (17) one immediately sees that the peak at the Higgs due to the first term of Eq. (17), and represented in Fig. 2 for the case $g = 0$, cancels out here with the second term. Thus, in this case the Higgs becomes visible only through its coupling to the phonon, but its direct visibility $\chi_{R\Delta}$ still influences the overall shape of the Raman spectra.

The crucial difference between the behavior of the Raman response and the behavior of the phonon propagator in a phonon-induced CDW transition has been completely overlooked in the previous work [18,19]. For example, the claim usually done [18,19] that the transfer of spectral weight between the two peaks in the phonon spectral function A_D must be found also in the Raman spectra is not correct. In general, this is not the case, as the comparison between the Figs. 6(a)–6(c) clearly demonstrates. This simple fact can also be used to explain the polarization dependence of the Higgs signatures reported recently in NbSe₂ [17]. Indeed, even though our model is not intended to give a realistic description of NbSe₂, nonetheless some general conclusions can be drawn from our results that can be used to interpret the Raman experiments. The general results of our calculations in the case of a phonon-mediated Higgs response can be summarized in two separate items. First, the overlap between the CDW and SC order parameter in part of the Fermi surface is necessary to give rise to a finite $\chi_{D\Delta}$ function in Eq. (16), that controls the effective coupling between the CDW phonon and the Higgs [see Eq. (15)]. In turn, larger is the fraction of Fermi surface where the overlap occurs and stronger is the enhancement of the Higgs mode itself, shown in Fig. 1, that helps its visibility. Second, both the phonon and the Higgs become Raman visible through intermediate electronic processes, given by χ_{RD} and $\chi_{R\Delta}$, respectively (see Fig. 3). These two functions depend on the combined symmetry of the (CDW or SC) gap and of the Raman light polarization. Thus, different Raman symmetry will give in general a different result since both functions will acquire a specific frequency and temperature dependence. As a consequence, the differences observed experimentally in NbSe₂ by means of the various Raman symmetries [17] can be used to extract specific information on the response functions χ_{RD} and $\chi_{R\Delta}$, and in turn on the gaps themselves.

IV. DISCUSSION AND CONCLUSIONS

This work focuses on two different problems: the nature of the Higgs mode in the coexisting CDW+SC state, and the issue of its detection in Raman spectroscopy. The first result, discussed in Sec. II, is that in the coexisting CDW+SC state the CDW gap pushes the quasiparticle excitations away from the Higgs pole. Thus, in contrast to the usual SC case, the Higgs mode presents a sharp spectral function, whose detection can be easier, whatever is the mechanism that couples it to a physical observable. It is also interesting that the power-law divergence of the amplitude fluctuations at twice the SC gap

value resembles the behavior of the Higgs mode predicted in relativistic $\mathcal{O}(N)$ theories [5–7], that are expected to work for superfluids or strongly coupled superconductors. A possible way to test directly our prediction could be, for example, an out-of-equilibrium optical experiment, where a nonlinear coupling of the current to the Higgs can be generated [15]. Indeed, in this case we expect that the strongly reduced damping of the Higgs mode in the coexisting state will lead to a much slower decay of the amplitude oscillations with respect to the conventional superconductors investigated so far [13,15]. It is worth noting that the mechanism outlined here can also have a potential impact on the detection of the Higgs mode in other families of superconductors. For example, in cuprate superconductors, where signatures of a $2\Delta_0$ oscillation in out-of-equilibrium spectroscopy have been also reported [14], the pseudogap in the quasiparticle excitations present already above T_c could contribute to enhance the Higgs fluctuations. Indeed, as mentioned above, a model similar to the one studied in this paper has been studied long ago as a simplified phenomenological description of a CDW-like pseudogap phase [32]. The quantitative effect on the Higgs should be, however, estimated within realistic models since in these materials the quasiparticle continuum extends up to zero frequency due to the d -wave nature of the order parameter. Finally, it can be worth exploring also the nature of the Higgs fluctuations in the coexisting spin-density-wave and superconducting state, a situation realized nowadays in some families of iron-based superconductors [38].

The second part of the paper focuses on the Raman detection of the Higgs mode. Here, the final results depend crucially on the nature of the CDW instability itself, as due to an electronic interaction or to the coupling to a phonon. In the former case, one probes directly the Higgs spectral function, so a signature at $2\Delta_0$ appears in the Raman response, while in the latter case the Higgs signature moves below $2\Delta_0$ due to the coupling to the phonon. In both cases, one sees that when damping effects, neglected in the previous literature [18,19], are taken into account, it is crucial to consider the modified nature of the Higgs mode in the coexisting state in order to resolve the Higgs signatures in the experiments. Moreover, we clarified how the Raman response depends crucially on the intermediate electronic processes that make the Higgs or the phonon Raman visible. This issue, that is often overlooked in the literature [4,18,19], explains the origin of the direct Raman visibility of the Higgs and the transfer of spectral weight between the phonon and Higgs peak. In particular, we suggest that our results can be used as a guideline to infer useful information on the still unsolved issue of the symmetry of the CDW and SC gaps in NbSe₂.

ACKNOWLEDGMENTS

We thank M. Méasson, C. Castellani, and J. Lorenzana for useful discussions and suggestions. We acknowledge financial support by MIUR under the projects FIRB-HybridNanoDev-RBFR1236VV, PRIN-RIDEIRON-2012X3YFZ2, and Progetto Premiale 2012-ABNANOTECH.

APPENDIX A: COUPLING OF THE HIGGS MODE TO RAMAN IN A LATTICE MODEL

In this Appendix, we clarify the role played by the intermediate electronic process $\chi_{R\Delta}$ that couples the Higgs mode to the Raman charge density [see Fig. 3(a)]. In particular, we show that at weak SC coupling the coupling of the SC amplitude fluctuations to the Raman charge fluctuations ($\chi_{R\Delta}$) or to the real charge fluctuations ($\chi_{\rho\Delta}$) can be different from each other. Such a difference is crucial since these two quantities play, as we shall see, a quite different role.

Let us first discuss the coupling of the Higgs mode to real charge fluctuations in an ordinary SC, i.e., without preformed CDW state. By means of the standard definition of charge operator $\rho(\mathbf{q}) \equiv \sum_{\mathbf{k}\sigma} c_{\mathbf{k}-\mathbf{q}/2,\sigma}^\dagger c_{\mathbf{k}+\mathbf{q}/2,\sigma}$, one can easily find the well-known [33,36] result that

$$\chi_{\rho\Delta} = \frac{4\Delta_0}{N} \sum_{\mathbf{k}} \frac{\xi_{\mathbf{k}} \tanh(\beta E_{\mathbf{k}}/2)}{E_{\mathbf{k}} [(i\Omega_n)^2 - 4E_{\mathbf{k}}^2]}, \quad (\text{A1})$$

where $\xi_{\mathbf{k}} = \varepsilon_{\mathbf{k}} - \mu$ is a generic band dispersion and $E_{\mathbf{k}} = \sqrt{\xi_{\mathbf{k}}^2 + \Delta_0^2}$. In the weak-coupling limit, the above integral is dominated by the region around the Fermi level $\xi_{\mathbf{k}} = 0$. As a consequence, for *any* band structure one can assume that the above integral vanishes because of the particle-hole symmetry of the integration limits enforced by the BCS solution, that allows one to put $\chi_{\rho\Delta} \simeq N_0 \Delta_0 \int_{-\infty}^{\infty} d\xi \xi / [\sqrt{\xi^2 + \Delta_0^2} (\omega^2 - 4\xi^2 - 4\Delta_0^2)] = 0$. In general, the particle-hole symmetry of the fermionic bubbles in the BCS limit is also evoked to guarantee that amplitude and charge/phase fluctuations are uncoupled at Gaussian level, as we mentioned above Eq. (3), allowing one to study the amplitude sector independently from the charge one. The situation is instead radically different at strong coupling, as discussed, e.g., in Refs. [33,36].

When one computes instead the coupling of the Higgs mode to the Raman charge fluctuations $\rho_R(\mathbf{q}) \equiv \sum_{\mathbf{k}\sigma} \Gamma(\mathbf{k}) c_{\mathbf{k}-\mathbf{q}/2,\sigma}^\dagger c_{\mathbf{k}+\mathbf{q}/2,\sigma}$ one should consider the additional momentum modulation of the charge provided by the polarization-dependent factor $\Gamma(\mathbf{k})$. Thus, even remaining within a BCS scheme $\chi_{R\Delta}$ can be different from zero even if $\chi_{\rho\Delta} \simeq 0$. This can be seen easily in our model, where the two quantities $\chi_{R\Delta}$ and $\chi_{\rho\Delta}$ at half-filling are given, respectively, by Eq. (10) and

$$\chi_{\rho\Delta} = \frac{4\Delta_0}{N} \sum_{\mathbf{k}} \frac{\varepsilon_{\mathbf{k}} \tanh(\beta E_{\mathbf{k}}/2)}{E_{\mathbf{k}} [(i\Omega_n)^2 - 4E_{\mathbf{k}}^2]}, \quad (\text{A2})$$

where now $E_{\mathbf{k}} = \sqrt{\varepsilon_{\mathbf{k}}^2 + \Delta_0^2 + D_0 \gamma_{\mathbf{k}}^2}$. As a consequence in our case, where the band structure is particle-hole symmetric, at half-filling $\chi_{\rho\Delta}$ is *exactly zero* and it remains negligibly small away from it. On the other hand, as we mentioned in the text, in the A_{1g} channel where $\Gamma(\mathbf{k}) = (\cos k_x + \cos k_y) \propto \varepsilon_{\mathbf{k}}$ the integral (10) that defines $\chi_{R\Delta}$ is finite. Indeed, for a constant CDW gap, Eq. (A2) at $T = 0$ can be approximately estimated as $\chi_{\rho\Delta} \sim \Delta_0 N_0 \int d\varepsilon \varepsilon / [\sqrt{\varepsilon^2 + R^2} (\omega^2 - 4\varepsilon^2 - 4R^2)] = 0$ while $\chi_{R\Delta} \sim \Delta_0 N_0 \int d\varepsilon \varepsilon^2 / [\sqrt{\varepsilon^2 + R^2} (\omega^2 - 4\varepsilon^2 - 4R^2)] \neq 0$, where $R^2 = \Delta_0^2 + D_0^2$. Notice that to appreciate this difference, it is crucial to retain a full lattice description of the problem, that has been neglected in the previous theoretical approach [18,19].

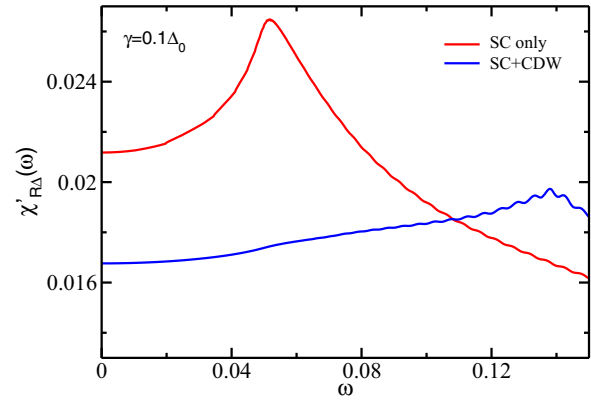


FIG. 7. (Color online) Real part of the Raman response function $\chi_{R\Delta}$ at $T = 0$ in the pure SC and in the coexistence SC+CDW state for a residual $\gamma = 0.1\Delta_0$, as in Figs. 1 and 2. As one can see, in the mixed CDW+SC case $\chi'_{R\Delta}$, that appears as a prefactor in the Raman susceptibility (11), is featureless at the frequency $2\Delta_0$ where the Higgs spectral function shown in Fig. 1(c) has a maximum.

In summary, in our description of the CDW+SC state, we can still safely neglect all the complications [33,36] of the coupling between the amplitude mode and the charge density one since we are still in a weak-coupling scheme where $\chi_{\rho\Delta} \simeq 0$ at all dopings, but we can retain a finite coupling of the Higgs to the Raman probe, encoded in $\chi_{R\Delta} \neq 0$. In this respect, the general claim done in Ref. [4] that the Higgs mode is decoupled by the Raman spectra because of particle-hole symmetry is formally uncorrect. However, it is still true that $\chi_{R\Delta}$ is a small quantity, so when the Higgs is an overdamped mode, as in an ordinary superconductor, the overall effect of amplitude fluctuations on the Raman response will be negligible (see dashed lines in Fig. 2). In the CDW+SC state instead the modifications of the Higgs spectral function A_{Δ} can make this small coupling $\chi_{R\Delta}$ crucial, leading to the strong Raman response represented by the solid lines in Fig. 2. We notice also that the enhancement of the Raman response in the mixed state occurs here despite the fact that $\chi_{R\Delta}$ itself is *smaller* in the coexisting state, as shown in Fig. 7, due to the presence of the CDW gap. In other words, as we emphasized above, the crucial role of the CDW for what concerns the Raman response is *not* to enhance the visibility itself of the Higgs, encoded in the electronic process $\chi_{R\Delta}$ (that is indeed even suppressed). The CDW changes crucially the nature of the Higgs spectral function, making the Higgs detectable even in the presence of a small coupling to the Raman light.

APPENDIX B: VARIATION OF THE HIGGS MODE WITH DOPING

To elucidate the effect of the CDW gap on the Higgs mode in the case where a larger part of the Fermi surface remains ungapped below T_{CDW} , we show here the analogous calculations of Fig. 2 of the paper away from half-filling. In our model, the CDW gap decreases when one moves away from half-filling, due to the lack of perfect nesting. If one keeps the SC coupling U fixed, this reflects also in a rapid increase of the SC order parameter at $T = 0$, as shown in Fig. 8(a). However,

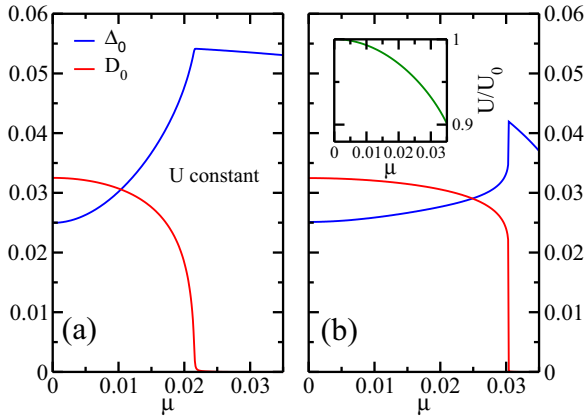


FIG. 8. (Color online) Doping variation of the CDW and SC gap at $T = 0$ in the case of a constant (a) or varying (b) SC coupling U . In (b) U decreases slightly with doping with respect to the value U_0 at $\mu = 0$ (see inset), in order to reproduce a weaker increase of Δ with doping.

in order to make the comparison between different dopings meaningful, we decided here to reduce also U with doping, in order to retain an almost constant SC gap [see Fig. 8(b)]. This allows one to compare the effects on the Higgs mode due only to the increase of the quasiparticle contribution starting at $2\Delta_0$, while keeping Δ_0 almost fixed.

As mentioned in Sec. II, when one moves away from half-filling the general form of the effective action is more complicated than Eq. (7) since one should retain in principle also the coupling of the amplitude mode at $\mathbf{q} = 0$ and \mathbf{Q} . One can then show that the Raman response reads as

$$\chi_{RR}(q) = [\mathcal{M}_{RR}^0(q) - \mathcal{M}_{\Delta R}(q)\mathcal{M}_{\Delta\Delta}^{-1}\mathcal{M}_{\Delta R}^T(-q)]_{11}, \quad (\text{B1})$$

where the matrices \mathcal{M}_{RR}^0 , $\mathcal{M}_{\Delta R}$, and $\mathcal{M}_{\Delta\Delta}$ correspond to the BCS term, to the Higgs-Raman coupling, and to the Higgs fluctuations, respectively, with

$$\mathcal{M}_{RR}^0(q) \equiv \begin{bmatrix} \Lambda_{3333}^{\Gamma\Gamma}(q) & \Lambda_{1333}^{\tilde{\Gamma}\Gamma}(q) \\ \Lambda_{3313}^{\Gamma\tilde{\Gamma}}(q) & \Lambda_{1313}^{\tilde{\Gamma}\tilde{\Gamma}}(q) \end{bmatrix}, \quad (\text{B2})$$

$$\mathcal{M}_{\Delta R}(q) \equiv \begin{bmatrix} \Lambda_{0133}^{\Gamma}(q) & \Lambda_{1133}^{\Gamma}(q) \\ \Lambda_{0113}^{\tilde{\Gamma}}(q) & \Lambda_{1113}^{\tilde{\Gamma}}(q) \end{bmatrix}, \quad (\text{B3})$$

$$\mathcal{M}_{\Delta\Delta}(q) \equiv \begin{bmatrix} \frac{2}{v} + \Lambda_{0101}(q) & \Lambda_{1101}(q) \\ \Lambda_{0111}(q) & \frac{2}{v} + \Lambda_{1111}(q) \end{bmatrix}. \quad (\text{B4})$$

The fermionic susceptibilities $\Lambda_{ijkl}(q)$ are defined as

$$\Lambda_{ijkl}(q) \equiv \frac{T}{N} \sum_k \text{Tr}[G_0(k+q)\sigma_i \otimes \sigma_j G_0(k)\sigma_k \otimes \sigma_l], \quad (\text{B5})$$

and the superscripts $\Gamma, \tilde{\Gamma}$ refer to the insertion of a Raman vertex $\Gamma(\mathbf{k})$ or $\tilde{\Gamma}(\mathbf{k}) \equiv \Gamma(\mathbf{k} + \mathbf{Q}/2)$.

The element $[\mathcal{M}_{\Delta\Delta}]_{11} \equiv X_{\Delta\Delta}$ corresponds at half-filling to the inverse Higgs propagator given by Eq. (5). Moreover, at $\mu = 0$ in the A_{1g} channel the off-diagonal elements of both $\mathcal{M}_{\Delta R}$ and $\mathcal{M}_{\Delta\Delta}$ vanish, and one is left with the Eq. (9) of

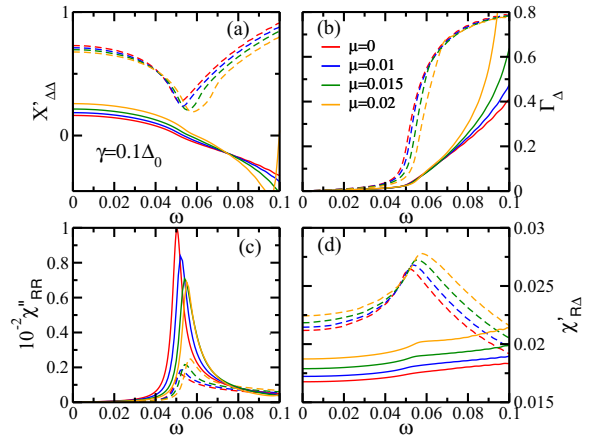


FIG. 9. (Color online) Frequency dependence of the real (a) and imaginary (b) parts of the inverse amplitude mode at $T = 0$ for different doping levels. In the CDW+SC state (solid lines) the gaps are taken from Fig. 8(b), while in the pure SC case (dashed lines) U is tuned to have the same Δ_0 at $T = 0$. The resulting Raman response is shown in panel (c), while panel (d) shows the Raman-Higgs coupling function, that is always smaller in the coexistence state.

Sec. II above. At $\mu \neq 0$, we computed the full expression (B1), even though we verified that the main contribution of the Higgs fluctuations to the Raman response comes from $X_{\Delta\Delta}$, whose real and imaginary parts are displayed in Figs. 9(a) and 9(b). As one can see, even though at finite filling a finite Fermi surface exists above T_c , leading to a larger contribution of the quasiparticle continuum above $2\Delta_0$, still the Higgs mode preserves a strong relativistic character near the pole, with a progressively larger damping above it. Thus, when one compares again the results in the pure SC and in the mixed CDW+SC state [Fig. 9(c)], in the latter case the Higgs spectral function leads to a stronger feature in Raman. In full analogy with the case of Fig. 2, this enhanced Raman response is not due to the prefactor, represented in the case of Eq. (B1) by the matrix $\mathcal{M}_{\Delta R}$, whose largest contribution $\chi_{RA} \equiv [\mathcal{M}_{\Delta R}]_{11}$ is shown in Fig. 9(d). Once more, the enhancement of the response in the mixed state reflects the enhancement of the Higgs fluctuations due to the preformed CDW gap, even when this leaves a larger part of the Fermi surface ungapped. We checked that the present results hold also when the Coulomb interaction is explicitly taken into account since both the BCS term \mathcal{M}_{RR}^0 and the screening term coming from charge fluctuations [34] are always much smaller than the contribution of the Higgs. Finally, we note that even though this paper is not intended to give a quantitative description of NbSe₂, the persistent anomalous character of the Higgs mode with doping shown in Fig. 9 is an encouraging suggestion that the same results will hold also with a more general band structure as the one of NbSe₂, where finite portions of the Fermi surfaces are ungapped by the CDW. In addition, Fig. 8(b) shares also some similarity with the experimental phase diagram under pressure of NbSe₂ [39,40], suggesting that the present approach could also be used in the future for a qualitative understanding of the evolution of the Raman spectra under pressure.

- [1] S. Weinberg, *The Quantum Theory of Fields, Vol. 2: Modern Applications* (Cambridge University Press, Cambridge, UK, 1996).
- [2] S. Dittmaier and M. Schumacher, *Prog. Nucl. Part. Phys.* **70**, 1 (2013).
- [3] N. Nagaosa, *Quantum Field Theory in Condensed Matter Physics* (Springer, New York, 1999).
- [4] For a recent review, see D. Pekker and C. M. Varma, [arXiv:1406.2968](https://arxiv.org/abs/1406.2968).
- [5] D. Podolsky, A. Auerbach, and D. P. Arovas, *Phys. Rev. B* **84**, 174522 (2011).
- [6] L. Pollet and N. Prokofev, *Phys. Rev. Lett.* **109**, 010401 (2012).
- [7] Snir Gazit, Daniel Podolsky, and Assa Auerbach, *Phys. Rev. Lett.* **110**, 140401 (2013).
- [8] U. Bissbort, S. Götze, Y. Li, J. Heinze, J. S. Krauser, M. Weinberg, C. Becker, K. Sengstock, and W. Hofstetter, *Phys. Rev. Lett.* **106**, 205303 (2011).
- [9] M. Endres, T. Fukuhara, D. Pekker, M. Cheneau, P. Schauss, C. Gross, E. Demler, S. Kuhr, and I. Bloch, *Nature (London)* **487**, 454 (2012).
- [10] A. F. Volkov and S. M. Kogan, *Zh. Eksp. Teor. Fiz.* **65**, 2038 (1973) [*Sov. Phys.-JETP* **38**, 1018 (1974)].
- [11] I. O. Kulik *et al.*, *J. Low. Temp. Phys.* **43**, 591 (1981).
- [12] T. Cea, D. Bucheli, G. Seibold, L. Benfatto, J. Lorenzana, and C. Castellani, *Phys. Rev. B* **89**, 174506 (2014).
- [13] Ryusuke Matsunaga, Yuki I. Hamada, Kazumasa Makise, Yoshinori Uzawa, Hiroataka Terai, Zhen Wang, and Ryo Shimano, *Phys. Rev. Lett.* **111**, 057002 (2013).
- [14] B. Mansarta, J. Lorenzana, A. Manna, A. Odehb, M. Scaronigella, M. Cherguib, and F. Carbone, *Proc. Natl. Acad. Sci. USA* **110**, 4539 (2013).
- [15] Ryusuke Matsunaga, Naoto Tsuji, Hiroyuki Fujita, Arata Sugioka, Kazumasa Makise, Yoshinori Uzawa, Hiroataka Terai, Zhen Wang, Hideo Aoki, Ryo Shimano, *Science* **345**, 1145 (2014).
- [16] R. Sooryakumar and M. V. Klein, *Phys. Rev. Lett.* **45**, 660 (1980); *Phys. Rev. B* **23**, 3213 (1981).
- [17] M.-A. Méasson, Y. Gallais, M. Cazayous, B. Clair, P. Rodière, and L. Cario, *and A. Sacuto Phys. Rev. B* **89**, 060503(R) (2014).
- [18] P. B. Littlewood and C. M. Varma, *Phys. Rev. B* **26**, 4883 (1982).
- [19] D. A. Browne and K. Levin, *Phys. Rev. B* **28**, 4029 (1983).
- [20] J. C. Tsang, J. E. Smith, and M. W. Shafer, *Phys. Rev. Lett.* **37**, 1407 (1976).
- [21] T. Yokoya, T. Kiss, A. Chainani, S. Shin, M. Nohara, and H. Takagi, *Science* **294**, 2518 (2001).
- [22] T. Valla, A. V. Fedorov, P. D. Johnson, P.-A. Glans, C. McGuinness, K. E. Smith, E. Y. Andrei, and H. Berger, *Phys. Rev. Lett.* **92**, 086401 (2004).
- [23] T. Kiss, T. Yokoya, A. Chainani, S. Shin, T. Hanaguri, M. Nohara, and H. Takagi, *Nat. Phys.* **3**, 720 (2007).
- [24] S. V. Borisenko, A. A. Kordyuk, V. B. Zabolotnyy, D. S. Inosov, D. Evtushinsky, B. Buchner, A. N. Yaresko, A. Varykhalov, R. Follath, W. Eberhardt, L. Patthey, and H. Berger, *Phys. Rev. Lett.* **102**, 166402 (2009).
- [25] D. J. Rahn, S. Hellmann, M. Kalläne, C. Sohrt, T. K. Kim, L. Kipp, and K. Rossnagel, *Phys. Rev. B* **85**, 224532 (2012).
- [26] E. Hanamura and N. Nagaosa, *Physica (Amsterdam)* **105B**, 400 (1981).
- [27] M. V. Klein, *Phys. Rev. B* **25**, 7192 (1982).
- [28] M. J. Rice, *Phys. Rev. Lett.* **37**, 36 (1976).
- [29] A. B. Kuzmenko, L. Benfatto, E. Cappelluti, I. Crassee, D. van der Marel, P. Blake, K. S. Novoselov, and A. K. Geim, *Phys. Rev. Lett.* **103**, 116804 (2009).
- [30] Z. Li, C. H. Lui, E. Cappelluti, L. Benfatto, K. F. Mak, G. L. Carr, J. Shan, and T. F. Heinz, *Phys. Rev. Lett.* **108**, 156801 (2012).
- [31] E. Cappelluti, L. Benfatto, M. Manzardo, and A. B. Kuzmenko, *Phys. Rev. B* **86**, 115439 (2012).
- [32] See, e.g., L. Benfatto, S. Caprara, and C. Di Castro, *Eur. Phys. J. B* **17**, 95 (2000); S. Chakravarty, R. B. Laughlin, D. K. Morr, and C. Nayak, *Phys. Rev. B* **63**, 094503 (2001).
- [33] For the usual SC case, see e.g. L. Benfatto, A. Toschi, and S. Caprara, *Phys. Rev. B* **69**, 184510 (2004) and references therein.
- [34] T. P. Deveraux and R. Hackl, *Rev. Mod. Phys.* **79**, 175 (2007).
- [35] M. J. Rice and S. Strässler, *Solid State Commun.* **13**, 1931 (1974); P. A. Lee, T. M. Rice, and P. W. Anderson, *ibid.* **14**, 703 (1974); **86**, 115439 (2012) and references therein.
- [36] Jan R. Engelbrecht, M. Randeria and C. A. R. Sá de Melo, *Phys. Rev. B* **55**, 15153 (1997).
- [37] To compare the results of Fig. 5 with the ones in Ref. [18] consider that the values $g_{\Delta} = 0.02$ and 0.04 used here correspond to the values $\alpha = 0.25$ and $\alpha \simeq 1$ of the dimensionless coupling α introduced by LV.
- [38] G. R. Stewart, *Rev. Mod. Phys.* **83**, 1589 (2011).
- [39] C. Berthier, P. Molinié, and D. Jérôme, *Solid State Commun.* **18**, 1393 (1976).
- [40] Y. Feng *et al.*, *Proc. Natl. Acad. Sci. USA* **109**, 7224 (2012).